

See discussions, stats, and author profiles for this publication at: <https://www.researchgate.net/publication/275894963>

# Graphene Nanoplatelets with Selectively Functionalized Edges as Electrode Material for Electrochemical Energy Storage

ARTICLE in LANGMUIR · MAY 2015

Impact Factor: 4.46 · DOI: 10.1021/acs.langmuir.5b00195 · Source: PubMed

---

CITATIONS

2

READS

102

## 6 AUTHORS, INCLUDING:



Dhrubajyoti Bhattacharjya

Korea University

22 PUBLICATIONS 438 CITATIONS

[SEE PROFILE](#)



Hyeanyeol Park

Korea University

7 PUBLICATIONS 57 CITATIONS

[SEE PROFILE](#)



Tandra Panja

Daegu Gyeongbuk Institute of Science and T...

5 PUBLICATIONS 2 CITATIONS

[SEE PROFILE](#)



Jong-Beom Baek

Ulsan National Institute of Science and Tech...

193 PUBLICATIONS 6,082 CITATIONS

[SEE PROFILE](#)

## Graphene Nanoplatelets with Selectively Functionalized Edges as Electrode Material for Electrochemical Energy Storage

Dhrubajyoti Bhattacharjya,<sup>†,‡</sup> In-Yup Jeon,<sup>§</sup> Hyean-Yeol Park,<sup>†,‡</sup> Tandra Panja,<sup>†</sup> Jong-Beom Baek,<sup>\*,§</sup> and Jong-Sung Yu<sup>\*,†</sup>

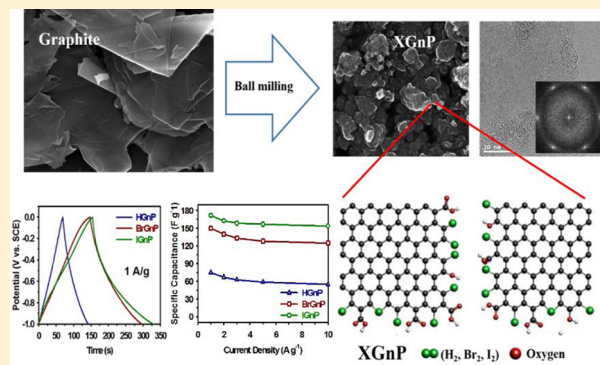
<sup>†</sup>Department of Energy Systems Engineering, Daegu Gyeongbuk Institute of Science and Technology (DGIST), Daegu, 711-873, Republic of Korea

<sup>‡</sup>Department of Advanced Materials Chemistry, Korea University, 2511 Sejong-ro, Sejong 339-700, Republic of Korea

<sup>§</sup>School of Energy and Chemical Engineering, Low-Dimensional Carbon Materials Center, Ulsan National Institute of Science and Technology (UNIST), UNIST-gil 50, Ulsan 689-798, Republic of Korea

### Supporting Information

**ABSTRACT:** In recent years, graphene-based materials have been in the forefront as electrode material for electrochemical energy generation and storage. Despite this prevalent interest, synthesis procedures have not attained three important efficiency requirements, that is, cost, energy, and eco-friendliness. In this regard, in the present work, graphene nanoplatelets with selectively functionalized edges (XGnPs) are prepared through a simple, eco-friendly and efficient method, which involves ball milling of graphite in the presence of hydrogen ( $H_2$ ), bromine ( $Br_2$ ), and iodine ( $I_2$ ). The resultant HGnP, BrGnP, and IGnP reveal significant exfoliation of graphite layers, as evidenced by high BET surface area of 414, 595, and  $772\text{ m}^2\text{ g}^{-1}$ , respectively, in addition to incorporation of H, Br, and I along with other oxygen-containing functional groups at the graphitic edges. The BrGnP and IGnP are also found to contain 4.12 and 2.20 at % of Br and I, respectively in the graphene framework. When tested as supercapacitor electrode, all XGnPs show excellent electrochemical performance in terms of specific capacitance and durability at high current density and long-term operation. Among XGnPs, IGnP delivers superior performance of  $172\text{ F g}^{-1}$  at  $1\text{ A g}^{-1}$  compared with  $150\text{ F g}^{-1}$  for BrGnP and  $75\text{ F g}^{-1}$  for HGnP because the large surface area and high surface functionality in the IGnP give rise to the outstanding capacitive performance. Moreover, all XGnPs show excellent retention of capacitance at high current density of  $10\text{ A g}^{-1}$  and for long-term operation up to 1000 charge–discharge cycles.



### INTRODUCTION

In recent years, electrochemical energy storage is one of the intensively pursued technological researches around the world. To compete with other conventional energy sources, an electrochemical energy storage system requires not only high performance in terms of capacity and durability but also environmental benignancy and cost efficiency.<sup>1,2</sup> In this context, supercapacitors have emerged as exciting development and have been a subject of intensive research efforts.<sup>3</sup> Supercapacitors are commonly used in consumer electronics, memory back-up systems, industrial power, and energy management.<sup>2,4</sup> There are two kinds of charge-storage mechanism that can be used for electrochemical energy storage. One involves faradaic charge transfer between electrode and electrolyte, as shown in pseudocapacitor or galvanic cell, whereas the other requires nonfaradaic charge accumulation on electrode/electrolyte interface, as seen in the electrical double-layer capacitor (EDLC). Faradaic nature of charge storage leads to high capacity and energy density in pseudocapacitors, but because of the slow nature of it, they are often handicapped by

low power density and poor cycle life. On the other hand, because of high reversibility of EDL formation at the electrode/electrolyte interface, EDLC has high power density ( $10^3$  to  $10^4\text{ W kg}^{-1}$ ), long cycle life ( $>10^6$  cycles), low maintenance cost, and better safety compared with LIBs.<sup>1–3,5,6</sup> In addition, the presence of functional groups on the electrode surface can take part in redox processes with electrolyte ions, which can supplement as pseudocapacitance to the EDL capacitance.<sup>1,7</sup>

Porous carbon materials, conducting polymers, transition-metal oxides, and sulfides are generally studied as electrode materials for supercapacitor.<sup>2,8–11</sup> Among them, porous carbon materials such as activated carbon (AC), hard carbon, ordered mesoporous carbon, graphene, and carbon nanotube (CNT) are the most attractive as electrode materials due to their high structural stability, polarizability, electrical conductivity, low cost, and versatile forms of existence such as powders, fibers,

Received: January 17, 2015

Revised: March 20, 2015

sheets, composites, tubes, and so on.<sup>2,3,7,8,12–15</sup> Moreover, high chemical inertness in different electrolytes (organic and inorganic) and broad thermal stability further enhance the attraction of carbon materials.<sup>6</sup> High surface area, surface morphology, pore size distribution, and presence of surface functional groups are main parameters for checking usability of carbon material as electrode material.<sup>16</sup> Numerous methods have been investigated to synthesize porous carbon materials such as sacrificial templating methods using silica or surfactant, catalytic activation by using metal salts or organometallic compounds, carbonization of polymer blends and aerogels, chemical activation, physical activation, flame synthesis, and so on;<sup>13,16–20</sup> however, as a result of ingesting expensive precursor, energy, as well as time, the evolution of simple low-cost strategies for synthesis of nanostructured carbon materials is still pursued extensively in research arena. Considering all of these parameters, ease of synthesis process and environmental benignity, graphene, and graphene-based materials have evolved as an excellent material for supercapacitor electrode.<sup>21–25</sup>

Graphene possesses high structural stability, unique morphology, superior electrical conductivity, and high specific surface area;<sup>26–28</sup> however, poor intrinsic capacitance of graphene has severely restricted its commercial viability for applications as electrode material.<sup>21,23,27</sup> Recently, extensive research has been carried out to introduce heteroatom into graphene structure for modulation of electron donor or acceptor properties in the molecular framework, which is likely to improve the specific capacity and cycle stability.<sup>29,30</sup> Various heteroatoms, such as boron (B), nitrogen (N), phosphorus (P), sulfur (S), and their mixtures have been studied as dopant for their influence in capacitive performance of doped graphene materials.<sup>31–38</sup> The difference in atomic size and electronegativity between the heteroatom and carbon in covalently doped graphitic carbon frameworks can polarize adjacent carbon atoms to introduce lattice defect and charge imbalance and thus create large numbers of surface active sites.<sup>32–34</sup> These active sites not only improve surface area but also enhance surface wettability with polar electrolyte ions. Therefore, most of the surfaces can be accessed by electrolyte ions for charge storage. Moreover, the heteroatoms can take part in reversible faradaic redox processes with electrolyte ions to supplement extra capacitance to the system.<sup>31,35</sup> So far, numerous methods have been employed to produce heteroatom-doped graphene materials, such as chemical vapor deposition (CVD), arc discharge, nitrogen plasma, high-temperature pyrolysis, solvothermal method, and so on;<sup>22,23,27,32,39</sup> however, all of these methods are either very expensive or involve environmentally hazardous reagents, and thus are not suitable for large-scale production. In recent times, high-energy ball milling has been widely explored as an eco-friendly and easily scalable method for the synthesis of graphene nanoplatelets.<sup>40–43</sup> Wang et al. have reported an amorphous carbonaceous material with high specific surface area synthesized by the ball milling and its application as electrode material for supercapacitor.<sup>44</sup> They have found that abundant oxygen functional groups (carboxyl and alkoxy) were introduced on graphite surface by the milling treatment, which significantly enhanced the electrochemical performance. Recently, Jeon et al. have shown that when the ball-milling process was performed in the presence of various chemical dopants regardless of the states of the dopant (such as gas, liquid and solid), it gave rise to high amount of exfoliation as well as induction of various functional groups such as H, Br,

I, and so on at the graphene edges.<sup>42,45,46</sup> The resultant functionalized graphene nanoplatelets (GnPs) were found to show dramatic increase in specific surface area without decreasing the surface conductivity substantially, in contrast with how it is generally observed in Hummers method.<sup>47</sup> Therefore, these GnPs materials are expected to have tremendous potential as electrode material for supercapacitor. Here the GnPs materials doped with each of three different dopants, namely, H, Br, and I, are used as electrode for supercapacitor, and their electrochemical properties are studied.

## EXPERIMENTAL SECTION

**Reagents and Materials.** Graphite was obtained from Alfa Aesar (Natural, –100 mesh, 99.9995% metals basis) and used as received. Hydrogen was purchased from Daesung Industrial Gases. Bromine ( $\text{Br}_2$ ) and iodine ( $\text{I}_2$ ) were purchased from Aldrich Chemical and used as received. All other solvents were supplied by Aldrich Chemical and used without further purification, unless otherwise specified.

**Synthesis of XGnPs.** XGnPs were prepared simply by ball-milling pristine graphite in the presence of  $\text{H}_2$ ,  $\text{Br}_2$ , and  $\text{I}_2$ , respectively. In a typical experiment, the pristine graphite (5.0 g) was placed in a stainless-steel capsule containing stainless-steel balls (500 g, diameter 5 mm). The capsule was then sealed and degassed after applying reduced pressure (0.05 mmHg) and then charged with  $\text{H}_2$  gas (10 bar), bromine ( $\text{Br}_2$ , 20 g), and iodine ( $\text{I}_2$ , 20 g). The capsule was then fixed in the planetary ball-mill machine and rotated with 500 rpm for 48 h. The resultant products were Soxhlet extracted with acetone to get rid of unreactive materials and were washed with 1.0 M aqueous HCl solution to remove metallic impurities, if any. Final products were then freeze-dried for 48 h to yield HGnPs (5.32 g), BrGnPs (6.93 g), and IGnPs (6.86 g) of dark black powder.

**Instrumentations.** The field-emission scanning electron microscopy (FE-SEM) was performed on FEI Nanonova 230 microscope operating at 30 kV, while the high-resolution transmission electron microscopy (HR-TEM) was carried out on a JEOL JEM-2100F (Cs) microscope operating at 200 kV. The TEM specimen was prepared by dipping carbon microgrids (Ted Pella, 200 Mesh Copper Grid) into well-dispersed samples in ethanol. X-ray photoelectron spectra (XPS) were recorded on a Thermo Fisher K-alpha XPS spectrometer. The surface area was measured by nitrogen adsorption–desorption isotherms using the Brunauer–Emmett–Teller (BET) method on Micromeritics ASAP 2504N. X-ray diffraction (XRD) patterns were recorded with a Rigaku D/MAXZ 2500 V/PC with Cu– $\text{K}\alpha$  radiation (35 kV, 20 mA,  $\lambda = 1.5418 \text{ \AA}$ ). Micro-Raman measurements were made with a WiTec Alpha300S system with 532 nm wavelength laser light and a 50× objective. Electrical conductivity measurements for all of the samples were performed using a home-built four-point probe apparatus as a function of applied pressure. Details of conductivity measurement process are given in the Supporting Information.

**Supercapacitor Cell Construction and Electrochemical Measurements.** All electrochemical characterizations of the synthesized XGnP ( $X = \text{H}, \text{Br}, \text{I}$ ) were performed in an electrochemical workstation (VSP, Biologic) using a conventional three-electrode configuration with 6.0 M aqueous KOH solution as electrolyte. 99.8% pure nickel foam with 2 mm thickness (MTI) was used to serve as a current collector. Platinum coil and saturated calomel electrode (SCE) were used as counter and reference electrode, respectively. The active material (XGnP) was mixed with a conducting agent (graphite) and binder (polyvinyl difluoride) in the weight ratio of 8:1:1, and a slurry was prepared by using 1-methyl-2-pyrrolidone as a solvent. The slurry was brush-coated on the Ni foam over a 1  $\text{cm}^2$  area and then dried overnight at room temperature, followed by another overnight drying in oven at 80 °C. These dried electrodes were then pressed at 3000 psi pressure. Approximately 4( $\pm 1$ ) mg of active materials was loaded in each electrode. The constructed cell was kept overnight to ensure proper wetting of electrodes by the electrolyte. The electrochemical measurements were carried out by cyclic voltammetry (CV) and galvanostatic charge–discharge (CD) and electrochemical impedance

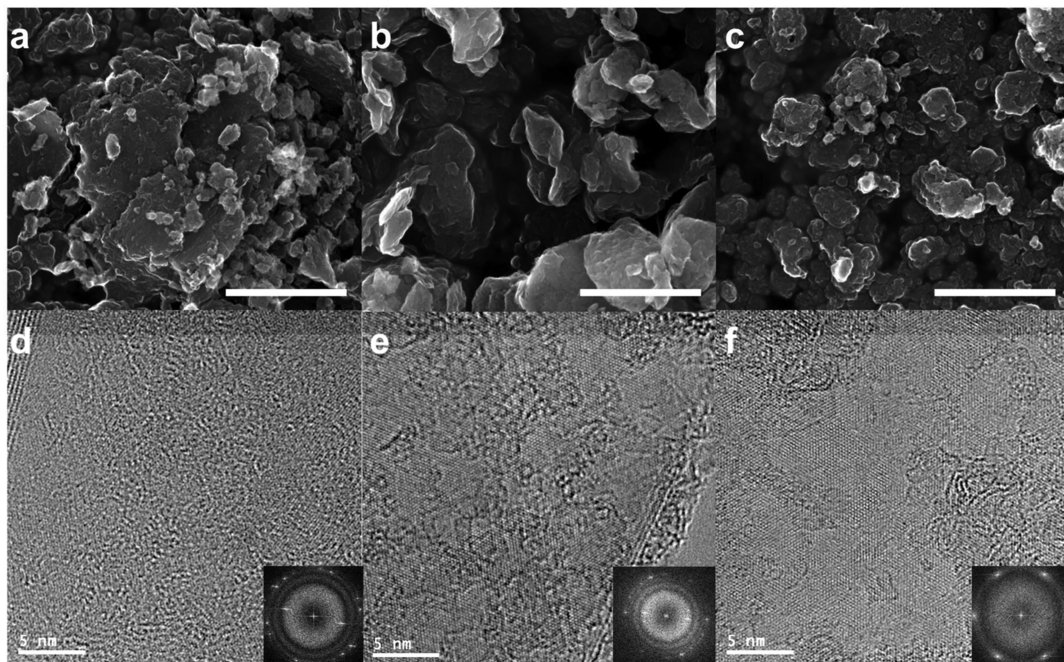


**Figure 1.** SEM images of XGnPs: (a) HGnP, (b) BrGnP, and (c) IGnP. Scale bars are 1  $\mu\text{m}$ . HR-TEM images of XGnPs: (d) HGnP, (e) BrGnP, and (f) IGnP. Insets are the selected area electron diffraction (SAED) patterns.

**Table 1. Element Content Measured from EDS and XPS Analyses and Porosity Measurement Data for the Pristine Graphite and XGnPs**

sample	atomic percentage				BET surface area ( $\text{m}^2 \text{ g}^{-1}$ )	pore volume ( $\text{cm}^3 \text{ g}^{-1}$ )	pore size (nm)
	C	O	Br	I			
graphite	EDS	98.80	1.20		3	0.0	2.3
	XPS	98.35	1.64				
HGnP	EDS	89.26	10.74		414	0.41	4.0
	XPS	86.15	13.85				
BrGnP	EDS	90.91	4.96	4.12	595	0.55	3.7
	XPS	88.99	8.42	2.59			
IGnP	EDS	88.22	9.57	2.20	772	0.73	3.8
	XPS	89.93	9.20	0.87			

(EIS) spectroscopy (EIS) methods. CV and CD for carbon materials in alkaline electrolyte were recorded in potential window of 0.0 to  $-1.0 \text{ V}$  versus SCE, where Ni foam is inert to any electrochemical reaction. EIS measurements were carried out in the frequency range of 10 kHz to 10 mHz with a 10 mV AC amplitude around 0.0 V versus open-circuit potential. The Nyquist plot obtained was fitted with an equivalent circuit using ZFit program to get the impedance parameters. The specific capacitance ( $C_{\text{SP}}$ ) was calculated from CD measurements using the following equation

$$C_{\text{SP}} = \frac{I \times t}{m \times V}$$

where  $I$  is the current,  $t$  is the time of discharge,  $m$  is the mass of the active material, and  $V$  is the potential window.

## RESULTS AND DISCUSSION

High-speed planetary motion (500 rpm) achieved in planetary ball-milling process produces sufficient energy to cause mechanochemical cleavage of graphitic C–C bonds. As a result, several types of active carbon species (mostly carboradicals, carbocations, and carbanions) can be generated at the broken edges of graphite. When these active carbon species come in contact with atmospheric oxygen, various functional groups such as carboxyl and alkoxy and so on can be

formed on graphite surface.<sup>44</sup> Therefore, in the presence of particular chemical dopants, it is possible to introduce various functional groups at the broken edges of graphite. Several dopants have been reported to be introduced in the broken edges of graphene nanoplatelets through this process.<sup>42,45,46,48,49</sup>

The mechanochemical delamination of graphite and formation of graphene nanoplatelets were confirmed from morphological investigations by using SEM and TEM. As compared with the pristine graphite with large plate-like morphology (Supporting Information Figure S1), SEM images of the resultant XGnPs show that all of XGnPs ( $X = \text{H, Br, I}$ ) have disordered morphology with small particle size in the range 0.1 to 1.0  $\mu\text{m}$  (Figure 1a–c). There is an obvious size reduction in all XGnPs ( $X = \text{H, Br, I}$ ) due to the mechanochemical exfoliation of graphite and in situ generation of small-sized active carbon pieces, which react with  $\text{H}_2$ ,  $\text{Br}_2$ , and  $\text{I}_2$  (Supporting Information Figure S2). The presence of Br and I is confirmed by energy-dispersive X-ray (EDX) spectroscopy (Supporting Information Figure S3 and Table 1) with elemental mapping (Supporting Information Figure S4). The atomic contents of Br and I are found to be 4.12 and 2.20 at % for BrGnP and IGnP, respectively.

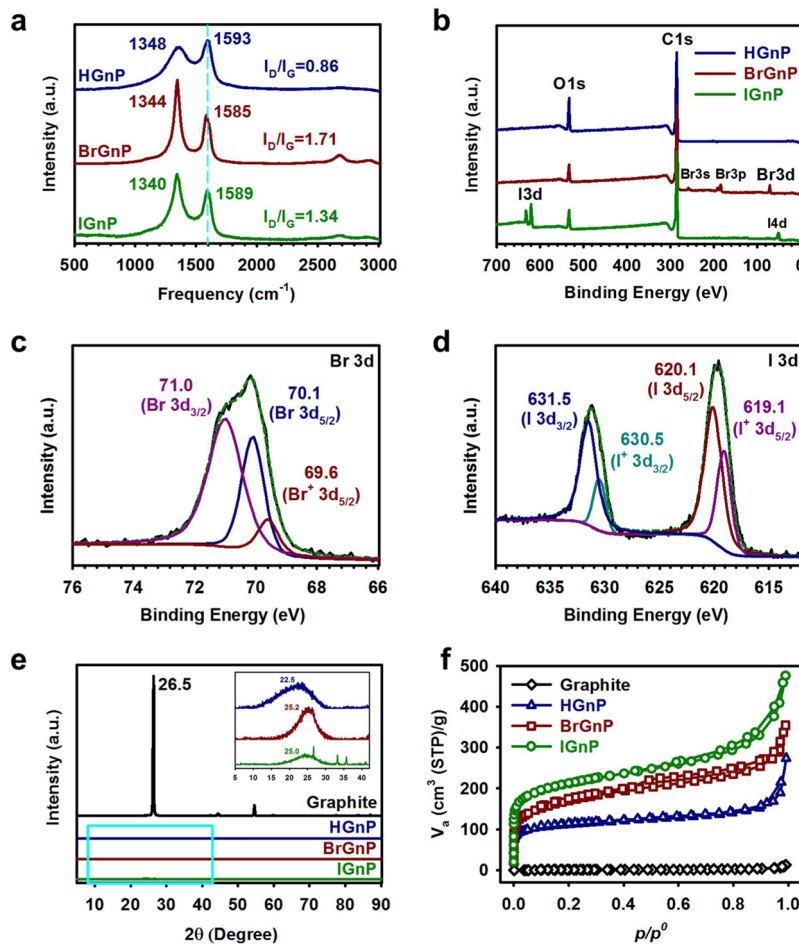


**Figure 2.** (a) Raman spectra and (b) XPS survey spectra for XGnPs along with deconvolution of high-resolution XPS peaks of (c) Br 3d for BrGnP and (d) I 3d for IGnP. (e) XRD patterns (inset: magnified blue area corresponding to (0 0 2) plane for the XGnPs) and (f) N<sub>2</sub> adsorption–desorption isotherms obtained 77K for XGnPs.

The HR-TEM images of XGnPs (Figure 1d–f) display graphene sheet morphologies where the graphitic lattice fringes on the basal plane are clearly visible along with some defects for BrGnP and IGnP. The lattice fringes are not distinct in the case of HGnP, which is probably due to higher density of defects on its basal plane than the other two. The selected area electron diffraction (SAED) patterns (inset of Figure 1d–f) also clearly show the honeycomb structure of graphitic lattice for all XGnPs. Therefore, the HR-TEM observation confirms that the graphitic structure is still preserved in the case of halogen functionalization despite the ball milling and workup procedure.

Raman spectroscopic analysis was carried out to analyze the structural defects created by the mechanochemical exfoliation and doping. As shown in Figure 2a, all XGnPs show strong D band at around 1350 cm<sup>-1</sup>, and  $I_D/I_G$  ratio for HGnP, BrGnP, and IGnP is found to be 0.86, 1.71, and 1.34, respectively. Although the  $I_D/I_G$  ratio for HGnP is much lower than its halogen functionalized counterparts probably due to its larger particle size (as seen in Figure 1a–c), it has broad D band unlike the other two. It signifies that HGnP has high density of defects, usually within the basal plane. The sharper D band and presence of 2D band for BrGnP and IGnP show that the basal plan is relatively intact, and the defects and functionalization occur selectively on the edges by halogen atoms with large atomic size and high electronegativity.<sup>50–52</sup> Moreover, the  $I_D/I_G$

$I_G$  ratio or D-band intensity for BrGnP is higher than that for IGnP because more Br gets grafted on the edge of graphene than I as supported by EDS and XPS (Table 1).

The functionalization of GnP were also confirmed by XPS measurements. In XPS survey spectrum of XGnPs (Figure 2b), Br 3s, Br 3p, and Br 3d peaks for BrGnP and I 3d and I 4d peaks for IGnP are observed, and the contents of Br and I are found to be 2.59 and 0.87 at % for BrGnP and IGnP, respectively, as summarized in Table 1. It can be mentioned here that the percentage composition of Br and I obtained from XPS analysis is lower than that obtained from EDS analysis. Despite the difference, similar trend in the Br and I atomic percentage is observed from both analyses. High-resolution XPS spectra of Br 3d and I 3d were also employed to study their electronic and bonding nature, as shown in Figure 2c,d. It can be observed that the spectra reveal combination of multiple peaks corresponding to the binding energies belonging to the ionic bonds (C–Br<sup>+</sup>–C and C–I<sup>+</sup>–C) and covalent bonds (C–Br and C–I) of bromine and iodine.<sup>45,53,54</sup> Although the ionic bond portion is smaller than the intact covalent binding portion, the former can enhance the electrochemical activity by taking part in faradaic redox process.

From the XRD patterns of XGnPs along with the pristine graphite as reference (Figure 2e), it can be observed that the pristine graphite shows a strong and sharp peak at 26.5° corresponding to (0 0 2) lattice plane with interlayer *d* spacing

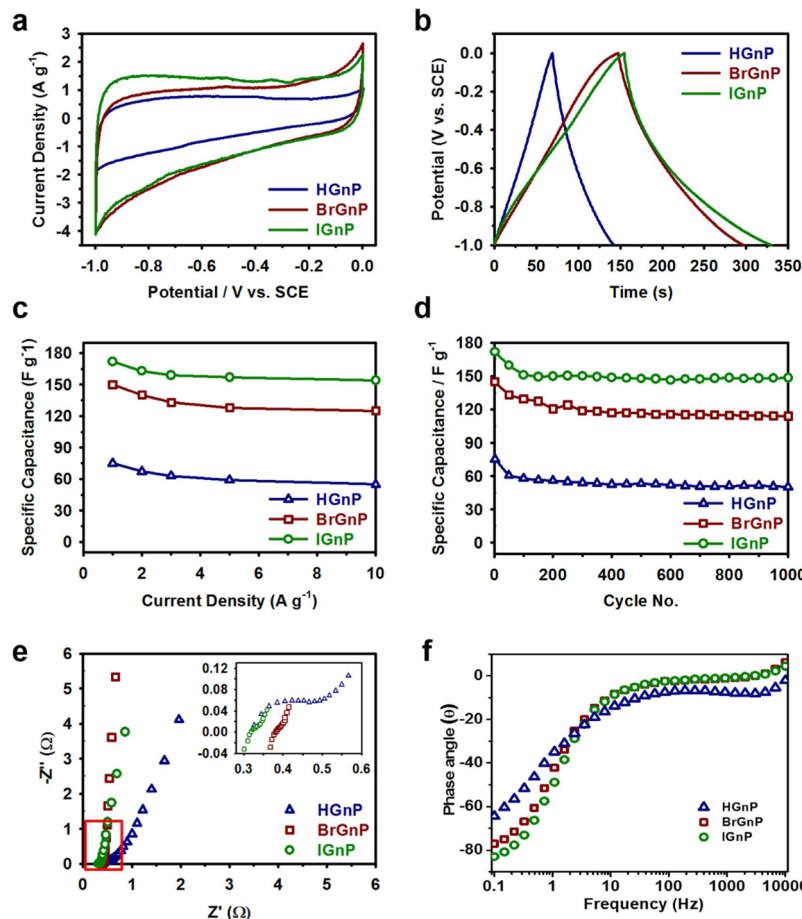


**Figure 3.** (a) Cyclic voltammograms at 5 mV s<sup>-1</sup> potential scan rate, (b) charge–discharge profiles at 1 A g<sup>-1</sup> current density, (c) specific capacitance at different current densities, (d) cyclic stability at 1 A g<sup>-1</sup> current density, (e) Nyquist plots, and (f) Bode plots for XGnPs.

of 0.34 nm. Compared with the pristine graphite, the main peaks of XGnPs are shifted to the left with negligible low intensity (<0.2% compared with that of the pristine graphite), indicating full delamination of most graphite layers via edge-selective functionalization during ball-milling process.<sup>32</sup> Unlike graphite oxide (GO), which shows large shift of (0 0 2) lattice plane to 10.2° due to random oxidation of lattice plane, Br-GnP and I-GnP show the corresponding peak at 25.0 and 25.2°, respectively (inset of Figure 2e). This indicates that the edges of XGnPs are mainly exfoliated and the distance between basal planes becomes broad due to grafted atoms, while the graphitic structure of basal plane is well maintained during ball milling and workup process. In the case of HGnP, the (0 0 2) lattice plane peak is shifted to 22.5°, indicating wider interlayer distance in it than those in the other halogen-functionalized GnP samples. This is probably due to the formation of amorphous structure at the edge of HGnP. Hydrogen can interact with active carbon species at the edge and generate sp<sup>3</sup> C–H bond, and thus the HGnP possesses bulky amorphous structures compared with BrGnP and IGnP systems, increasing the interlayer distance. Additionally, a few small but sharp peaks can be observed in the XRD spectrum of IGnP, which are probably originated from the use of stainless-steel ball-milling apparatus. because I<sub>2</sub> is highly corrosive toward stainless steel, a small amount of metal/metal oxide species may have remained trapped between IGnP layers, which could not be removed.

In N<sub>2</sub> adsorption–desorption isotherms for XGnPs (Figure 2f), it can be observed that all XGnPs show similar pattern, that

is, type I curve at low-relative pressures and type IV with a hysteresis at high pressures, which are typically associated with micropores and mesopores. The large surface area and coexistence of micropores and mesopores in XGnPs along with the ionic bonds (C–Br<sup>+</sup>–C and C–I<sup>+</sup>–C) can be beneficial for electrochemical activity of XGnPs. The porosity parameters obtained from N<sub>2</sub> sorption analysis (Table 1) show that the pristine graphite has very low specific surface area (SSA, BET-N<sub>2</sub>-method, 2.8 m<sup>2</sup> g<sup>-1</sup>) due to its highly ordered graphitic structure; however, after ball milling, the SSA of HGnP, BrGnP, and IGnP increases with 414.1, 595.2, and 772.0 m<sup>2</sup> g<sup>-1</sup>, respectively, which indicate a dramatic increase of about 148, 213, and 276 times, respectively, compared with that of the pristine graphite. This is because of extensive exfoliation of graphite layers by shear force as well as by wedging effect of heteroatom grafted at the edge of XGnPs. The shear force is well known and makes an important contribution to initial exfoliation process. The separation effect as wedge by grafted heteroatom is also significant for further exfoliation, making different surface area depending on the type of dopant. Because single-layer graphene has a theoretical SSA of 2630 m<sup>2</sup> g<sup>-1</sup>, the average number of graphene layers of XGnPs can be calculated as 6.4 (2630/414.1) for HGnP, 4.4 (2630/595.2) for BrGnP, and 3.4 (2630/772.0) for IGnP, suggesting that significant delamination of graphite layers occurs by ball milling.

The halogen functionality and large surface area obtained by edge-selective functionalization can be beneficial for electrochemical capacitive performance.<sup>56</sup> The electrochemical behav-

iors of XGnP were tested in a three-electrode configuration using 6.0 M aqueous KOH as electrolyte. As shown in Figure 3a, the comparative CV curves for all XGnP at 5 mV s<sup>-1</sup> potential scan rate demonstrate typical rectangular CV profiles pertaining to electrical double-layer formation. It can be observed that BrGnP and IGnP show more CV area coverage, that is, more specific capacitance than HGnP, which is due to higher specific surface area of BrGnP and IGnP than that of HGnP. Moreover, the polarization resistance is also lower for BrGnP and IGnP than that of HGnP, which can be visualized from the shift from ideally vertical change of current density on altering the electrode polarity near 0 and -1.0 V.<sup>20</sup> This shift is more evident in CVs carried out at higher scan rates (Supporting Information, Figure S5), and it signals the amount of intrinsic resistivity of the electrode material. Therefore, it can be assumed that the presence of halogen functionality imparts more electronic conductivity of the material.<sup>45</sup> The electronic conductivity of IGnP and BrGnP was measured to be 2.5 and 1.4 S cm<sup>-1</sup> at 19.5 MPa pressure, whereas it is 0.09 S cm<sup>-1</sup> for HGnP, as shown in Figure S6 of Supporting Information. Moreover, first-principle density-functional calculations also demonstrated that halogenated graphene edges can provide decent adsorption sites for aqueous electrolyte ion, which can eventually result in higher charge storage in BrGnP and IGnP.<sup>45</sup>

Figure 3b shows charge–discharge curves measured at 1 A g<sup>-1</sup> current density, which also demonstrate the performances similar to the CV measurement. The specific capacitance of HGnP, BrGnP, and IGnP were measured to be 75, 150, and 172 F g<sup>-1</sup>, respectively. This high specific capacitance showed by BrGnP and IGnP is due to not only the high surface area of them but also the high edge functionalities imparted by mechanochemical reaction of Br<sub>2</sub> and I<sub>2</sub> with graphite. It is recently reported that EDL capacitance of edge sites is more than basal plane sites.<sup>57</sup> Moreover, the presence of edge functionalities can also contribute additional quantum capacitance due to enhancement in density of states.<sup>58</sup> The difference in surface area may be a decisive factor for the small difference in specific capacitance between BrGnP and IGnP. However, the low specific capacitance of HGnP is due not only to its low surface area but also to low electronic conductivity.

The most important specification of a commercial supercapacitor is its excellent durability at high current density as well as for long-term operation. These two properties were also measured for XGnP electrodes (Figure 3c,d), and it was found that all XGnP show good performance in both aspects, with IGnP being the best in both criteria, which is followed by BrGnP and HGnP. In terms of durability for current density, HGnP, BrGnP, and IGnP display specific capacitance of 55, 125, and 154 F g<sup>-1</sup> at current density of 10 A g<sup>-1</sup>, which correspond to 73, 83, and 90% retention of values at 1 A g<sup>-1</sup>, respectively. In terms of long-term operation durability, HGnP, BrGnP, and IGnP display specific capacitance of 50, 114, and 148 F g<sup>-1</sup> after 1000 cycles of charge–discharge at 1 A g<sup>-1</sup>, which indicate 67, 79, and 86% retention, respectively.

Because the capacitance is always accompanied by resistance parameters, EIS spectroscopy is a good tool for measuring these parameters, and they are generally represented by Nyquist plot and Bode plot.<sup>59,60</sup> It can be observed from the resultant Nyquist plots in Figure 3e, wherein BrGnP and IGnP show similar semicircle radius, while HGnP reveals larger semicircle radius. This semicircle represents the charge-transfer resistance and arises due to intrinsic resistivity of the electrode material.<sup>20</sup> These are in good accordance with the electronic

conductivity data of XGnP samples, as previously mentioned. Moreover, the Warburg resistance, which can be visualized in the Nyquist curve by the extent of deviation toward the x axis at the end of semicircle, is also found to be much higher for HGnP than its competitors. The Nyquist plots are simulated with probable circuit elements with the help of ZFit program, as shown in the Supporting Information Figure S7, and the resultant data are provided in Table 2. A more detailed

**Table 2. EIS Parameters of XGnP Obtained from Analysis of Nyquist Plot**

	HGnP	BrGnP	IGnP
R <sub>s</sub> (Ω)	0.33	0.38	0.30
C <sub>i</sub> (F·s <sup>1/α</sup> )	0.004 ( $α = 0.79$ )	0.85 ( $α = 0.55$ )	1.31 ( $α = 0.46$ )
R <sub>ct</sub> (Ω)	0.166	0.048	0.053
W (Ω·s <sup>-1/2</sup> )	1.088	0.147	0.357
C (mF)	201	310	464

explanation of the circuit diagram accompanied by electrical double layer can be found in the Supporting Information and also in previous literature.<sup>20,61</sup> The Bode plots in Figure 3f show the phase angle of BrGnP and IGnP electrode reaching almost 78 and 84° at 100 mHz AC frequency, which is very close to phase angle of ideal capacitor, that is, 90°. This is because of high electronic conductivity of IGnP, followed by BrGnP, whereas the phase angle for HGnP is only 65° at 100 mHz AC frequency, which shows a high number of resistive elements associated with this electrode.

## CONCLUSIONS

In summary, graphene nanoplatelets were prepared with selectively functionalized edges through an easy and cost-effective process, which involved reactive ball milling of graphite in the presence of hydrogen (H<sub>2</sub>), bromine (Br<sub>2</sub>), and iodine (I<sub>2</sub>). The resultant HGnP, BrGnP, and IGnP showed near complete exfoliation of graphite, as evidenced by high specific surface area as well as induction of H, Br, and I along with other oxygen-containing functional groups at the edges. As a result, XGnP showed excellent performances as electrode material for supercapacitor. IGnP demonstrated the highest performance followed by BrGnP and HGnP in terms of not only specific capacity but also durability to work at high current load and for long-time operation. This behavior can be clearly understood from the synergistic effect of large surface area and the presence of edge functional groups. Overall, the IGnP holds excellent potential to be a commercially viable electrode material for energy storage because the synthesis process is highly cost-effective, green, and easily upgradable to industrial-scale synthesis.

## ASSOCIATED CONTENT

### Supporting Information

Additional characterization data from SEM, EDS, EA, and cyclic voltammograms of XGnP. The Supporting Information is available free of charge on the ACS Publications website at DOI: 10.1021/acs.langmuir.5b00195.

## AUTHOR INFORMATION

### Corresponding Authors

\*J.-B.B.: E-mail: jbaek@unist.ac.kr.

\*J.-S.Y.: E-mail: jsyu@dgist.ac.kr. Tel: (+82) 53-785-6443. Fax: (+82) 53-785-6409.

## Notes

The authors declare no competing financial interest.

## ACKNOWLEDGMENTS

This research was supported by National Research Foundation (NRF) grant (NRF-2010-0029245), Global Frontier R&D Program on Center for Multiscale Energy System (NRF-2011-0031571), Mid-Career Researcher (MCR), and Basic Research Laboratory (BRL), and Basic Science Research programs through NRF funded by the Ministry of Education, Science and Technology of Korea. We also thank KBSI at Jeonju, Daejeon, and Chuncheon for SEM, TEM, and XPS measurements.

## REFERENCES

- (1) Wang, G.; Zhang, L.; Zhang, J. A review of electrode materials for electrochemical supercapacitors. *Chem. Soc. Rev.* **2012**, *41* (2), 797–828.
- (2) Arico, A. S.; Bruce, P.; Scrosati, B.; Tarascon, J.-M.; van Schalkwijk, W. Nanostructured materials for advanced energy conversion and storage devices. *Nat. Mater.* **2005**, *4* (5), 366–377.
- (3) Candelaria, S. L.; Shao, Y.; Zhou, W.; Li, X.; Xiao, J.; Zhang, J.-G.; Wang, Y.; Liu, J.; Li, J.; Cao, G. Nanostructured carbon for energy storage and conversion. *Nano Energy* **2012**, *1* (2), 195–220.
- (4) Stein, A.; Wang, Z.; Fierke, M. A. Functionalization of Porous Carbon Materials with Designed Pore Architecture. *Adv. Mater.* **2009**, *21* (3), 265–293.
- (5) Kötz, R.; Carlen, M. Principles and applications of electrochemical capacitors. *Electrochim. Acta* **2000**, *45* (15–16), 2483–2498.
- (6) Pandolfo, A. G.; Hollenkamp, A. F. Carbon properties and their role in supercapacitors. *J. Power Sources* **2006**, *157* (1), 11–27.
- (7) Simon, P.; Gogotsi, Y. Materials for electrochemical capacitors. *Nat. Mater.* **2008**, *7* (11), 845–854.
- (8) Chaudhari, N. K.; Chaudhari, S.; Yu, J.-S. Cube-like  $\alpha$ -Fe<sub>2</sub>O<sub>3</sub> supported on ordered multimodal porous carbon as high performance electrode material for supercapacitor. *ChemSusChem* **2014**, *7* (11), 3102–3111.
- (9) Rui, X.; Tan, H.; Yan, Q. Nanostructured metal sulfides for energy storage. *Nanoscale* **2014**, *6* (17), 9889–9924.
- (10) Jiang, J.; Li, Y.; Liu, J.; Huang, X.; Yuan, C.; Lou, X. W. Recent Advances in Metal Oxide-based Electrode Architecture Design for Electrochemical Energy Storage. *Adv. Mater.* **2012**, *24* (38), 5166–5180.
- (11) Kang, D.-Y.; Kim, S.-O.; Chae, Y. J.; Lee, J. K.; Moon, J. H. Particulate Inverse Opal Carbon Electrodes for Lithium-Ion Batteries. *Langmuir* **2013**, *29* (4), 1192–1198.
- (12) Zhang, L. L.; Zhao, S.; Tian, X. N.; Zhao, X. S. Layered Graphene Oxide Nanostructures with Sandwiched Conducting Polymers as Supercapacitor Electrodes. *Langmuir* **2010**, *26* (22), 17624–17628.
- (13) Bhattacharjya, D.; Kim, M.-S.; Bae, T.-S.; Yu, J.-S. High performance supercapacitor prepared from hollow mesoporous carbon capsules with hierarchical nanoarchitecture. *J. Power Sources* **2013**, *244* (0), 799–805.
- (14) Kim, M.-S.; Bhattacharjya, D.; Fang, B.; Yang, D.-S.; Bae, T.-S.; Yu, J.-S. Morphology-dependent Li storage performance of ordered mesoporous carbon as anode material. *Langmuir* **2013**, *29* (22), 6754–6761.
- (15) Saha, D.; Li, Y.; Bi, Z.; Chen, J.; Keum, J. K.; Hensley, D. K.; Grappe, H. A.; Meyer, H. M.; Dai, S.; Paranthaman, M. P.; Naskar, A. K. Studies on Supercapacitor Electrode Material from Activated Lignin-Derived Mesoporous Carbon. *Langmuir* **2014**, *30* (3), 900–910.
- (16) Fang, B.; Kim, J. H.; Kim, M.-S.; Yu, J.-S. Hierarchical Nanostructured Carbons with Meso-Macroporosity: Design, Characterization, and Applications. *Acc. Chem. Res.* **2013**, *46* (7), 1397–1406.
- (17) Nishihara, H.; Kyotani, T. Templatized Nanocarbons for Energy Storage. *Adv. Mater.* **2012**, *24* (33), 4473–4498.
- (18) Kim, J. H.; Fang, B.; Song, M. Y.; Yu, J.-S. Topological Transformation of Thioether-Bridged Organosilicas into Nanostructured Functional Materials. *Chem. Mater.* **2012**, *24* (12), 2256–2264.
- (19) Chaudhari, N. K.; Song, M. Y.; Yu, J.-S. Heteroatom-doped highly porous carbon from human urine. *Sci. Rep.* **2014**, *4*, 5221.
- (20) Bhattacharjya, D.; Yu, J.-S. Activated carbon made from cow dung as electrode material for electrochemical double layer capacitor. *J. Power Sources* **2014**, *262* (0), 224–231.
- (21) Pumera, M. Electrochemistry of graphene: new horizons for sensing and energy storage. *Chem. Rec.* **2009**, *9* (4), 211–223.
- (22) Pumera, M. Graphene-based nanomaterials for energy storage. *Energy Environ. Sci.* **2011**, *4* (3), 668–674.
- (23) Brownson, D. A. C.; Kampouris, D. K.; Banks, C. E. An overview of graphene in energy production and storage applications. *J. Power Sources* **2011**, *196* (11), 4873–4885.
- (24) Shuvo, M. A. I.; Khan, M. A. R.; Karim, H.; Morton, P.; Wilson, T.; Lin, Y. Investigation of Modified Graphene for Energy Storage Applications. *ACS Appl. Mater. Interfaces* **2013**, *5* (16), 7881–7885.
- (25) Raccichini, R.; Varzi, A.; Passerini, S.; Scrosati, B. The role of graphene for electrochemical energy storage. *Nat. Mater.* **2015**, *14*, 271–279.
- (26) Chen, J.; Li, C.; Shi, G. Graphene Materials for Electrochemical Capacitors. *J. Phys. Chem. Lett.* **2013**, *4* (8), 1244–1253.
- (27) Kamat, P. V. Graphene-Based Nanoassemblies for Energy Conversion. *J. Phys. Chem. Lett.* **2011**, *2* (3), 242–251.
- (28) Whitby, R. L. D. Chemical Control of Graphene Architecture: Tailoring Shape and Properties. *ACS Nano* **2014**, *8* (10), 9733–9754.
- (29) Dai, L. Functionalization of Graphene for Efficient Energy Conversion and Storage. *Acc. Chem. Res.* **2012**, *46* (1), 31–42.
- (30) Choi, H.-J.; Jung, S.-M.; Seo, J.-M.; Chang, D. W.; Dai, L.; Baek, J.-B. Graphene for energy conversion and storage in fuel cells and supercapacitors. *Nano Energy* **2012**, *1* (4), 534–551.
- (31) Wu, Z.-S.; Ren, W.; Xu, L.; Li, F.; Cheng, H.-M. Doped Graphene Sheets As Anode Materials with Superhigh Rate and Large Capacity for Lithium Ion Batteries. *ACS Nano* **2011**, *5* (7), 5463–5471.
- (32) Razmjooei, F.; Singh, K. P.; Song, M. Y.; Yu, J.-S. Enhanced electrocatalytic activity due to additional phosphorous doping in nitrogen and sulfur-doped graphene: A comprehensive study. *Carbon* **2014**, *78*, 257–267.
- (33) Singh, K. P.; Bae, E. J.; Yu, J.-S. Fe–P: a new class of electroactive catalyst for oxygen reduction reaction. *J. Am. Chem. Soc.* **2015**, *137*, 3165–3168.
- (34) Lazar, P.; Zboril, R.; Pumera, M.; Otyepka, M. Chemical nature of boron and nitrogen dopant atoms in graphene strongly influences its electronic properties. *Phys. Chem. Chem. Phys.* **2014**, *16* (27), 14231–14235.
- (35) Nasini, U. B.; Bairi, V. G.; Ramasahayam, S. K.; Bourdo, S. E.; Viswanathan, T.; Shaikh, A. U. Phosphorous and nitrogen dual heteroatom doped mesoporous carbon synthesized via microwave method for supercapacitor application. *J. Power Sources* **2014**, *250* (0), 257–265.
- (36) Ambrosi, A.; Poh, H. L.; Wang, L.; Sofer, Z.; Pumera, M. Capacitance of p- and n-Doped Graphenes is Dominated by Structural Defects Regardless of the Dopant Type. *ChemSusChem* **2014**, *7* (4), 1102–1106.
- (37) Hardikar, R. P.; Das, D.; Han, S. S.; Lee, K.-R.; Singh, A. K. Boron doped defective graphene as a potential anode material for Li-ion batteries. *Phys. Chem. Chem. Phys.* **2014**, *16* (31), 16502–16508.
- (38) Yun, Y. S.; Le, V.-D.; Kim, H.; Chang, S.-J.; Baek, S. J.; Park, S.; Kim, B. H.; Kim, Y.-H.; Kang, K.; Jin, H.-J. Effects of sulfur doping on graphene-based nanosheets for use as anode materials in lithium-ion batteries. *J. Power Sources* **2014**, *262* (0), 79–85.
- (39) Jung, S.-M.; Lee, E. K.; Choi, M.; Shin, D.; Jeon, I.-Y.; Seo, J.-M.; Jeong, H. Y.; Park, N.; Oh, J. H.; Baek, J.-B. Direct Solvothermal Synthesis of B/N-Doped Graphene. *Angew. Chem., Int. Ed.* **2014**, *53* (9), 2398–2401.

- (40) Chen, Y.; Fitz Gerald, J.; Chadderton, L. T.; Chaffron, L. Nanoporous carbon produced by ball milling. *Appl. Phys. Lett.* **1999**, *74* (19), 2782–2784.
- (41) Welham, N. J.; Berbenni, V.; Chapman, P. G. Effect of extended ball milling on graphite. *J. Alloys Compd.* **2003**, *349* (1–2), 255–263.
- (42) Chang, D. W.; Choi, H.-J.; Jeon, I.-Y.; Baek, J.-B. Edge-Selectively Functionalized Graphene Nanoplatelets. *Chem. Rec.* **2013**, *13* (2), 224–238.
- (43) Zhao, W.; Fang, M.; Wu, F.; Wu, H.; Wang, L.; Chen, G. Preparation of graphene by exfoliation of graphite using wet ball milling. *J. Mater. Chem.* **2010**, *20* (28), 5817–5819.
- (44) Wang, Y.; Cao, J.; Zhou, Y.; Ouyang, J.-H.; Jia, D.; Guo, L. Ball-Milled Graphite as an Electrode Material for High Voltage Supercapacitor in Neutral Aqueous Electrolyte. *J. Electrochem. Soc.* **2012**, *159* (5), A579–A583.
- (45) Jeon, I. Y.; Choi, H. J.; Choi, M.; Seo, J. M.; Jung, S. M.; Kim, M. J.; Zhang, S.; Zhang, L.; Xia, Z.; Dai, L.; Park, N.; Baek, J. B. Facile, scalable synthesis of edge-halogenated graphene nanoplatelets as efficient metal-free electrocatalysts for oxygen reduction reaction. *Sci. Rep.* **2013**, *3*, 1810.
- (46) Jeon, I. Y.; Choi, H. J.; Jung, S. M.; Seo, J. M.; Kim, M. J.; Dai, L.; Baek, J. B. Large-scale production of edge-selectively functionalized graphene nanoplatelets via ball milling and their use as metal-free electrocatalysts for oxygen reduction reaction. *J. Am. Chem. Soc.* **2013**, *135* (4), 1386–1393.
- (47) Hummers, W. S.; Offeman, R. E. Preparation of Graphitic Oxide. *J. Am. Chem. Soc.* **1958**, *80* (6), 1339–1339.
- (48) Park, J.-S.; Lee, M.-H.; Jeon, I.-Y.; Park, H.-S.; Baek, J.-B.; Song, H.-K. Edge-Exfoliated Graphites for Facile Kinetics of Delithiation. *ACS Nano* **2012**, *6* (12), 10770–10775.
- (49) Leon, V.; Quintana, M.; Herrero, M. A.; Fierro, J. L. G.; Hoz, A. d. l.; Prato, M.; Vazquez, E. Few-layer graphenes from ball-milling of graphite with melamine. *Chem. Commun.* **2011**, *47* (39), 10936–10938.
- (50) Cançado, L.; Pimenta, M.; Neves, B.; Dantas, M.; Jorio, A. Influence of the Atomic Structure on the Raman Spectra of Graphite Edges. *Phys. Rev. Lett.* **2004**, *93* (24), 247401.
- (51) Graf, D.; Molitor, F.; Ensslin, K.; Stampfer, C.; Jungen, A.; Hierold, C.; Wirtz, L. Spatially Resolved Raman Spectroscopy of Single- and Few-Layer Graphene. *Nano Lett.* **2007**, *7* (2), 238–242.
- (52) Kudin, K. N.; Ozbas, B.; Schniepp, H. C.; Prud'homme, R. K.; Aksay, I. A.; Car, R. Raman Spectra of Graphite Oxide and Functionalized Graphene Sheets. *Nano Lett.* **2007**, *8* (1), 36–41.
- (53) Zheng, Q. B.; Gudarzi, M. M.; Wang, S. J.; Geng, Y.; Li, Z.; Kim, J.-K. Improved electrical and optical characteristics of transparent graphene thin films produced by acid and doping treatments. *Carbon* **2011**, *49* (9), 2905–2916.
- (54) Buelow, M. T.; Gellman, A. J. The Transition State for Metal-Catalyzed Dehalogenation: C—I Bond Cleavage on Ag(111). *J. Am. Chem. Soc.* **2001**, *123* (7), 1440–1448.
- (55) Dikin, D. A.; Stankovich, S.; Zimney, E. J.; Piner, R. D.; Dommett, G. H. B.; Evmenenko, G.; Nguyen, S. T.; Ruoff, R. S. Preparation and characterization of graphene oxide paper. *Nature* **2007**, *448* (7152), 457–460.
- (56) Tanaike, O.; Yamada, Y.; Yamada, K.; Kodama, M.; Hatori, H.; Miyajima, N. Electrochemical behavior of halogen-doped carbon materials as capacitor electrodes. *ECS Trans.* **2011**, *33* (27), 71–76.
- (57) Yuan, W.; Zhou, Y.; Li, Y.; Li, C.; Peng, H.; Zhang, J.; Liu, Z.; Dai, L.; Shi, G. The edge- and basal-plane-specific electrochemistry of a single-layer graphene sheet. *Sci. Rep.* **2013**, *3*, 2248.
- (58) Pak, A. J.; Paek, E.; Hwang, G. S. Impact of Graphene Edges on Enhancing the Performance of Electrochemical Double Layer Capacitors. *J. Phys. Chem. C* **2014**, *118* (38), 21770–21777.
- (59) Taberna, P. L.; Simon, P.; Fauvarque, J. F. Electrochemical Characteristics and Impedance Spectroscopy Studies of Carbon-Carbon Supercapacitors. *J. Electrochem. Soc.* **2003**, *150* (3), A292–A300.
- (60) Orazem, M. E.; Tribollet, B. Electrical Circuits. In *Electrochemical Impedance Spectroscopy*; John Wiley & Sons, Inc.: New York, 2008; pp 61–72.
- (61) Luo, X.; Davis, J. J. Electrical biosensors and the label free detection of protein disease biomarkers. *Chem. Soc. Rev.* **2013**, *42* (13), 5944–5962.